RSC Advances

PAPER

View Article Online
View Journal | View Issue



Cite this: *RSC Adv.*, 2020, **10**, 44361

# Pretreatment by recyclable $Fe_3O_4$@Mg/Al-$CO_3$-LDH magnetic nano-adsorbent to dephosphorize for the determination of trace $F^-$ and $Cl^-$ in phosphorus-rich solutions

Si Chen,[ab] Yongchun Xu,[ab] Yu Tang,[ab] Wei Chen,*[ab] Shubin Chen,[ab] Lili Hu[ab] and Georges Boulon[c]

The magnetic nano-adsorbent $Fe_3O_4$@Mg/Al-$CO_3$-LDH (Mg/Al-type layered double hydroxide) with a $CO_3^{2-}$ interlayer anion has been synthesized successfully on $Fe_3O_4$ nanoparticles *via* a urea hydrothermal method. It is confirmed that the nano-adsorbent can adsorb $PO_4^{3-}$ rapidly and efficiently in multi-ion solutions; meanwhile, it did not adsorb any $F^-$ and $Cl^-$, even with a high amount of the nano-adsorbent or a longer adsorption time. This behaviour is beneficial for applications to remove $PO_4^{3-}$ in phosphorus-rich solutions, and especially can be utilized to determine trace $F^-$ and $Cl^-$ anions in phosphorus-rich solutions by physical and chemical analysis methods including ion chromatography without serious interference from $PO_4^{3-}$ for trace determinations. Herein, the hydrothermally synthesized $Fe_3O_4$@Mg/Al-$CO_3$-LDH was characterized *via* SEM, TEM, SAED, XRD, FTIR, magnetic hysteresis loop analysis and adsorption–desorption isotherm analysis. The structure and stability, adsorption mechanism, magnetic saturation value, specific surface area, total pore volume, phosphate adsorption capacity and recyclability are discussed. Using the optimized pretreatment conditions, $Fe_3O_4$@Mg/Al-$CO_3$-LDH was utilized successfully to adsorb $PO_4^{3-}$ in real samples and determine trace $F^-$ and $Cl^-$ accurately by ion chromatography; this would be very beneficial for continuous analysis and on-line tests by physical and chemical analysis methods without interference from $PO_4^{3-}$ in phosphorus-rich samples, leaving $F^-$ and $Cl^-$ even if in a trace content.

Received 10th September 2020
Accepted 6th November 2020

DOI: 10.1039/d0ra07761e

rsc.li/rsc-advances



## 1 Introduction

Currently, phosphate materials or its hybrid materials, presented as crystal, glass or ceramics, are widely applied[1] in numerous fields such as optics and electronics, as well as medical biomaterials for applications[2] in bone grafting and regeneration, drug delivery, *etc.* However, in the determination of target ions in solutions containing these materials, the matrix phosphate anion $PO_4^{3-}$ seriously interferes in determinations by methods such as spectrophotometry,[3] neutron activation,[4] molecular absorption spectrometry,[5] graphite furnace,[6] electrothermal atomic absorption spectrometry,[7] and inductively coupled plasma mass spectrometry.[8] To determine anion impurities, the commonly used chromatography method will be affected seriously by interference from the phosphate anion. The signal from a high concentration $PO_4^{3-}$ will cover the peak or deform the peak shape of the target anion.[9–11] Furthermore, it will make the analytical column overloaded, which will shorten the service life of the column. Once the analytical column is overloaded, a ghost peak will appear, or the next injection may not even be allowed.[11] Although solutions with a high concentration of $PO_4^{3-}$ can be diluted greatly, this also reduces the content of the target anion, leading to a content much lower than the detection limit.[10] After fully rinsing the loops[11] of the chromatograph for several runs using deionized water, a certain amount of $PO_4^{3-}$ as carryover resulting from the previous injection may still be observed even if a blank sample is used. Therefore, an appropriate sample pretreatment to dephosphorize solutions with a high $PO_4^{3-}$ content is particularly important.[10,11]

A further issue is specifically related to the determination of trace $F^-$ and $Cl^-$ anions in phosphorus-rich solutions. If $F^-$ anions from the raw materials and products of the phosphate industry such as from phosphate ore, phosphate fertilizer, phosphogypsum enter the biological chain continuously during manufacturing processes, storage and utilization, the bioaccumulated $F^-$ will pose a serious threat to human life. Thus, it is necessary to monitor trace $F^-$ and $Cl^-$ anions in phosphorus-

[a]*Key Laboratory of Materials for High Power Laser, Shanghai Institute of Optics and Fine Mechanics, Chinese Academy of Sciences, Shanghai 201800, China. E-mail: weichen@siom.ac.cn*

[b]*Center of Materials Science and Optoelectronics Engineering, University of Chinese Academy of Sciences, Beijing 100049, China*

[c]*Institut Lumière Matière (ILM), UMR5306 CNRS-Université Claude Bernard Lyon 1, Université de Lyon, 69622 Villeurbanne, France*

rich raw materials and final products.[12] Moreover, hydroxyapatite is a particularly promising bone-grafting material for dental and orthopaedic applications. The addition of trace $F^-$ can construct a microenvironment favouring bone healing and bone regeneration,[13] but its trace amount must be strictly controlled to avoid cell death or necrosis.[14] Thus, all the above-mentioned factors make the accurate determination of trace $F^-$ and $Cl^-$ in phosphorus-rich solutions necessary, with the aim to fully keep $F^-$ and $Cl^-$ and adsorb $PO_4^{3-}$ as much as possible during the pretreatment, which should be developed.

Layered double hydroxides (LDHs) are two-dimensional nanostructured anionic clays, with the general formula of $[M_{1-x}^{2+}M_x^{3+}(OH)_2]^{x+}[A_{x/n}^{n-}yH_2O]^{x-}$, where M is a metal cation and A is the interlayer anion with *n*-valence.[15,16] Strong chemical bonds exist within the layer of $[M_{1-x}^{2+}M_x^{3+}(OH)_2]^{x+}$, but the bonds between the interlayer anion of $[A_{x/n}^{n-}yH_2O]^{x-}$ and the layer of $[M_{1-x}^{2+}M_x^{3+}(OH)_2]^{x+}$ are relatively weak. This makes LDHs promising ion-exchangers[17] for applications to adsorb the $PO_4^{3-}$ anion.[17–30]

To efficiently adsorb $PO_4^{3-}$, the interlayer anion choice will play a key role. Based on LDHs, there are some good options to use the $Cl^-$ anion,[17,20,22–24,31] or $NO_3^-$ anion,[19,21,32] or $Cl^-$ and $SO_4^{2-}$ anions[25] as the interlayer anion. They can be used to adsorb $PO_4^{3-}$ effectively, but their adsorption efficiencies are inevitably affected by carbon dioxide ($CO_2$) or carbonate ($CO_3^{2-}$) from the preparation process of the LDH, the solution environment and even the atmosphere.[17,19,25]

Employing $CO_3^{2-}$ as the interlayer anion, Zn–Al-LDH,[18] Zr-modified MgFe-LDH($CO_3$),[27] $Fe_3O_4$@Mg–Al-LDH,[26] Mg–Fe LDH[28] and $Fe_3O_4$@gelatin-encapsulated hydrotalcite[33] were prepared to adsorb $PO_4^{3-}$ successfully by a co-precipitation method. By comparison, the hydrothermal method is a better way to prepare LDH with the $CO_3^{2-}$ interlayer anion using urea, which can well control the size and crystallinity of the prepared nanoparticle.[15] In the investigations for the preparation of LDH with $CO_3^{2-}$ *via* the urea hydrolysis method,[29,30,34–54] only two LDHs have been used as a phosphate adsorbent.[29,30] Cu–Al LDH (CuAl/biomass carbon fibre-layered double hydroxide)[29] was synthesized at 110 °C for 12 h, and Zn–Al LDHs[30] were synthesized at 150 °C for 36 h.

Herein, an Mg–Al LDH was hydrothermally synthesized with $Mg(NO_3)_2$, $Al(NO_3)_3$, and urea, using $CO_3^{2-}$ as the interlayer anion. To utilize magnetic solid phase extraction (MSPE), which can achieve the purpose of phosphate adsorption and its rapid separation, $Fe_3O_4$ magnetic nanoparticles were introduced into the Mg–Al LDH nano-adsorbent during the hydrothermal synthetic process. Using the prepared $Fe_3O_4$@Mg/Al-$CO_3$-LDH magnetic nano-adsorbent, adsorption–determination and recycle procedures were conducted, as described in Section 2.3. As described in Section 3.1, its structural properties were characterized *via* SEM, TEM, FTIR, and XRD, and its magnetic property, specific surface area, and porosity were also analysed. After optimizing the pretreatment conditions, as discussed in Section 3.2, the stability and recyclability after 15 cycles with high adsorption capacity is shown in Section 3.3. More importantly, it was found that the hydrothermally synthesized $Fe_3O_4$@Mg/Al-$CO_3$-LDH magnetic nano-adsorbent only adsorbed $PO_4^{3-}$, not $F^-$ and $Cl^-$ in solution. This is undoubtedly beneficial to accurately determine the content of $F^-$ and $Cl^-$ in phosphate solutions by chromatography, and the practical applications are introduced in Section 4.

# 2 Experimental

## 2.1 Hydrothermally synthesized $Fe_3O_4$@Mg/Al-$CO_3$-LDH

The magnetic layered double hydroxide nano-adsorbent $Fe_3O_4$@Mg/Al-$CO_3$-LDH was synthesized *via* a urea hydrothermal method. After several trials, 0.6 g of $Fe_3O_4$ nanoparticles (ultrafine powder purchased from Macklin) was used and added to 15 mL solution of 0.1 mol $L^{-1}$ NaOH (AR grade). After the mixture was dispersed by ultrasonication for 10 min, it was separated using a magnet for further use. Then 2.044 g $Mg(NO_3)_2\cdot 6H_2O$ (AR grade), 1.500 g $Al(NO_3)_3\cdot 9H_2O$ (AR grade), and 1.68 g urea ($CH_4N_2O$, AR grade) were added to 70 mL deionized water (Millipore Milli-Q Direct 8). The mixed salt solution was further mixed using a vortex mixer (NP-30S) for 15 min. The activated $Fe_3O_4$ and mixed salt solution were transferred to an autoclave and mixed for 2 h using the vortex mixer. Then the autoclave was heated at 120 °C for 12 h. Next, the autoclave was cooled to room temperature. The obtained product was separated by a magnet and washed with deionized water and ethanol (AR grade) three times, followed by drying in an oven at 60 °C for 12 h. Finally, the $Fe_3O_4$@Mg/Al-$CO_3$-LDH magnetic nano-adsorbent was obtained.

## 2.2 Instruments

SEM analysis was performed using an Inspect F50 field-emission scanning electron microscope (FEI) with a resolution of 2.0 nm. An acceleration voltage of 10 kV was applied during secondary electron imaging.

TEM analysis was performed using a JEM-2100F high-resolution field-emission transmission electron microscope (JEOL) with a point resolution of 0.24 nm and line resolution of 0.10 nm. To observe the morphology of the nanoparticles, the bright-field mode was utilized. To observe the electron diffraction from different regions on the nanoparticle, the selected area mode was utilized. An acceleration voltage of 200 kV was applied for both modes. The nanoparticles were dispersed by ethanol to form a suspending liquid before observation.

FTIR spectra were measured using a Nicolet Nexus Fourier transform infrared spectrometer (Thermo Fisher), in the range of 4000 to 400 $cm^{-1}$ with a resolution of 4 $cm^{-1}$. The nanoparticles were mixed with KBr (SP grade) in the mass ratio of 1 : 100. After grinding in an agate mortar, the mixture was pressed into a thin disc sample.

XRD patterns were collected using a SmartLab9 X-ray diffractometer (Rigaku) with Cu-K$\alpha$ radiation of $\lambda$ = 0.15418 nm in the $2\theta$ range of 0.08–78° with the scanning step of 0.02° and the step time of 2 s.

Magnetic hysteresis loop analysis was performed using a SQUID vibrating sample magnetometer (Quantum Design) in the magnetic field range of ±30 000 Oe.

Specific surface area and porosity were fitted from the $N_2$ adsorption–desorption isotherms, which were determined at 77

 

K using an ASAP 2460 Accelerated Surface Area and Porosimeter System (Micromeritics).

The contents of $F^-$, $Cl^-$, and $PO_4^{3-}$ were determined using an ICS 5000+ ion chromatograph (Thermo Fisher) with a 25 μL sample loop and a conductivity detector. An IonPac® AS18 (250 mm × 4.0 mm i.d.) was applied as the anion exchange analytical column, which was protected by the guard column of IonPac® AG18 (50 mm × 4.0 mm i.d.). The temperature of the column compartment was set to 30 °C. For the eluent of NaOH solution, the flow rate through the anion exchange analytical column was 1.00 mL $min^{-1}$, and its concentration was automatically adjusted by an electrolytic eluent generator. When the test time was set to 35 min, the eluent concentration would be 25 mmol (0–13 min), 40 mmol (13–30 min), and 25 mmol (30–35 min). Manual injection was done in the operation.

### 2.3 Adsorption–determination and recycle procedures

The two main procedures are exhibited in Fig. 1 to adsorb $PO_4^{3-}$ in a solution of $Fe_3O_4$@Mg/Al-$CO_3$-LDH for the determination of $F^-$ and $Cl^-$, and to recycle and reuse $Fe_3O_4$@Mg/Al-$CO_3$-LDH.

Specifically, 50 mg of the synthesized magnetic nano-adsorbent was added to 80 mL of sample solution. They were mixed in a beaker by a vortex mixer for 5 min. After the adsorbent was isolated from the suspension with a magnet, the residual solution was filtered using a 0.22 μm membrane. It was bubbled with $N_2$ for 30 s to remove $CO_3^{2-}$, and then passed through an OnGuard II H column to remove the metal cations. At this time, the residual solution after adsorption on the $Fe_3O_4$@Mg/Al-$CO_3$-LDH nanoparticles could be introduced into the ion chromatograph to determine $F^-$ and $Cl^-$.

For the recycle procedure, the used $Fe_3O_4$@Mg/Al-$CO_3$-LDH was collected and placed in 15 mL desorption solution, 5 wt% NaOH and 10 wt% $Na_2CO_3$ (AR grade), and further mixed using a vortex mixer for 30 min. With the aid of a magnet, the $Fe_3O_4$@Mg/Al-$CO_3$-LDH nanoparticles were washed with deionized water and ethanol three times. This was followed by drying in an oven at 60 °C for 12 h, and then $Fe_3O_4$@Mg/Al-$CO_3$-LDH was regenerated for use for a new cycle adsorption. It should be noted that NaOH in the desorption solution will not affect the stability of Mg/Al-$CO_3$-LDH since it was synthesized in an environment of NaOH, as indicated in Section 2.1.

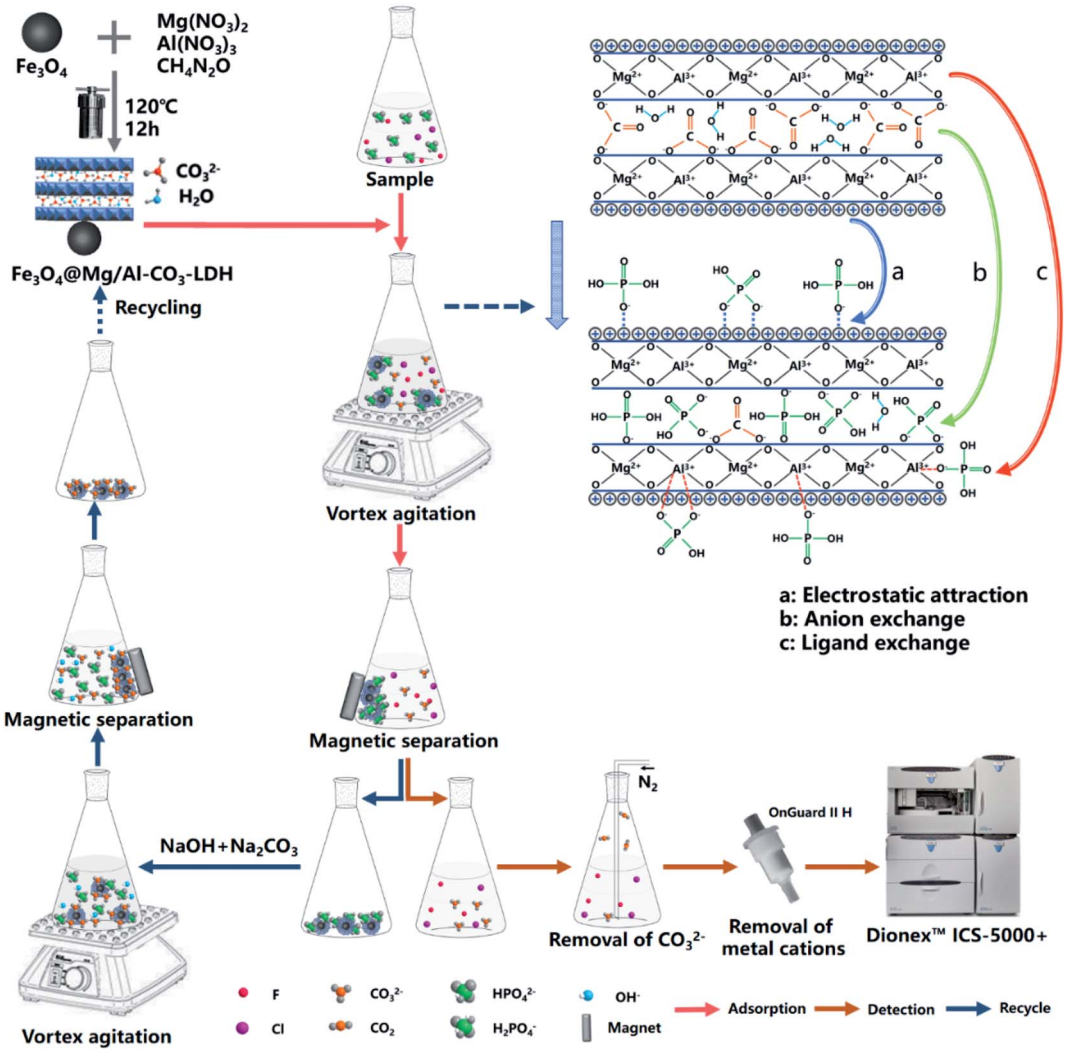


Fig. 1 Schematic illustration of the synthesis, adsorption, determination and recycle processes.

To evaluate the recyclability of the magnetic adsorbent, the phosphate adsorption capacity per unit mass of $Fe_3O_4$@Mg/Al-$CO_3$-LDH was measured for each cycle. Briefly, 50 mg of the magnetic adsorbent was added to 80 mL mixed solution with 1.00 mg $L^{-1}$ $F^-$, 1.00 mg $L^{-1}$ $Cl^-$ and $C_0 = 100$ mg P per L $PO_4^{3-}$ (based on P). Then, it was processed by 60 min mixing/adsorption, magnetic solid phase extraction–separation, filtering, bubbling, cation removal and chromatographic determination, as stated above. After determining the remaining phosphate concentration, $C_e$, which is also the equilibrium $PO_4^{3-}$ concentration in the solution, the adsorption capacity, $Q_e$, of $PO_4^{3-}$ was calculated by $Q_e = (C_0 - C_e)V/m$, where $V$ is the solution volume in L and $m$ is the dry weight of the nano-adsorbent in g.

# 3 Results and discussion

## 3.1 Characterization of $Fe_3O_4$@Mg/Al-$CO_3$-LDH

Fig. 2 shows the electron microscopy analysis of $Fe_3O_4$ and the synthesized $Fe_3O_4$@Mg/Al-$CO_3$-LDH magnetic nanoparticles. Both the SEM and bright-field TEM images show that $Fe_3O_4$ is an octahedral nanoparticle with clear edges and smooth surface, and its size is about 120 nm, as shown in Fig. 2(a) and (b). On the surface of $Fe_3O_4$, Mg/Al-$CO_3$-LDH was synthesized *via* the urea hydrothermal method. The shape of these irregular $Fe_3O_4$@Mg/Al-$CO_3$-LDH nanoparticles is not like the octahedron of $Fe_3O_4$, and on their surface, some protuberances exist, as shown in Fig. 2(c). According to the bright-field TEM image shown in Fig. 2(d), these protuberances also can be observed at the outer boundary of the bright gray region, and the bright gray region surrounding the dark region of $Fe_3O_4$ is characterized by a flake-like matrix. This is similar to the morphology of $Fe_3O_4$@CuMgAl-LDH nanoparticles.[55] Due to the stacking of many small flakes, the hydrothermally synthesized Mg/Al-$CO_3$-LDH on $Fe_3O_4$ nanoparticles appears to consist of an agglomeration of plate-like structures.[56]

Fig. 3(a) shows the high-resolution TEM image of the synthesized $Fe_3O_4$@Mg/Al-$CO_3$-LDH, where the bottom-left dark region and the bottom-right bright region were chosen for SAED, as shown in Fig. 3(b) and (c), respectively. The selected area electron diffraction (SAED) for the dark region clearly shows 4.910 Å, 3.193 Å, 2.469 Å and 1.698 Å diffractions, corresponding to the (111), (220), (222) and (422) planes of $Fe_3O_4$ (PDF card: #19-0629). Also, the SAED for the bright region shows 1.541 Å and 1.476 Å diffractions, corresponding to the (110) and (113) planes of Mg/Al-LDH (PDF card: #89-0460). Although the diffraction spots for the bright region are somewhat blurred, as shown in Fig. 3(c), the hexagonal diffraction pattern can still be observed, which is the typical diffraction pattern of LDH crystals.[55]

Thus, the above electron microscopic analysis indicates that during the hydrothermal process, $Fe_3O_4$ retains its original crystalline state, and Mg/Al-LDH is grown as small crystal plates. Their crystallization is also indicated by the XRD pattern shown in Fig. 4(a) for as-synthesized $Fe_3O_4$@Mg/Al-$CO_3$-LDH. The diffraction peaks at the $2\theta$ values of 18.24° (111), 30.08° (220), 35.46° (311), 37.04° (222), 43.12° (400), 53.50° (422), 57.04° (511), and 62.56° (400) correspond to the octahedral $Fe_3O_4$ crystal,[26] and the peaks at the $2\theta$ values of 11.54° (003), 23.44° (006), 35.46° (012), 61.02° (110), and 62.56° (113) correspond to the Mg–Al-LDH crystal.[26,57] More importantly, after 15 cycles of $PO_4^{3-}$-adsorption and regeneration of $Fe_3O_4$@Mg/Al-$CO_3$-LDH, as stated in Section 2.3, both the XRD peak positions and intensities remained almost unchanged, as shown in Fig. 4(a) and (b). This indicates that even after 15 cycles, the

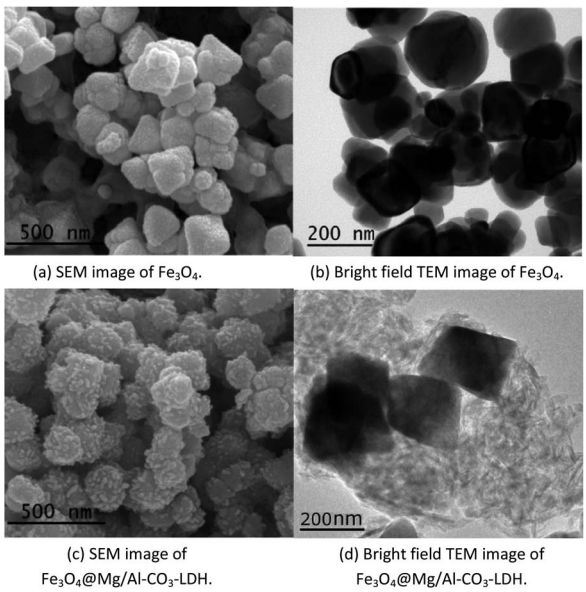


Fig. 2 Electron microscopy analysis of $Fe_3O_4$ nanoparticles and prepared $Fe_3O_4$@Mg/Al-$CO_3$-LDH magnetic nano-adsorbent.

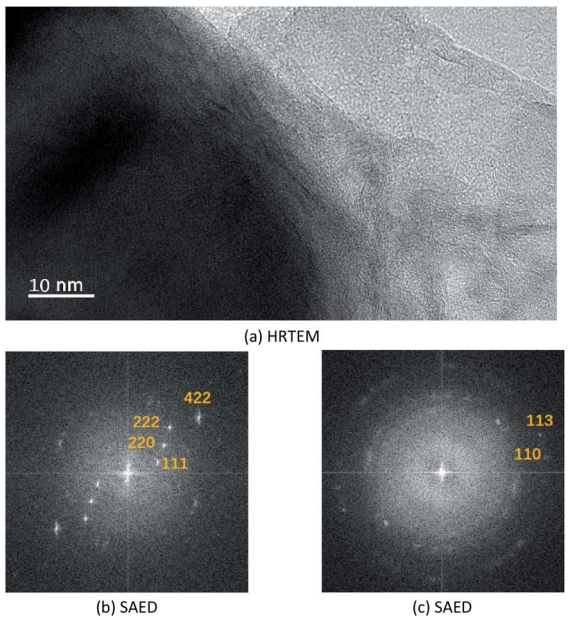


Fig. 3 High-resolution transmission electron microscopy (HRTEM) and selected area electron diffraction (SAED) for prepared $Fe_3O_4$@Mg/Al-$CO_3$-LDH, where (b) corresponds to the area at the bottom-left of (a), and (c) corresponds to the area at the bottom-right of (a).

 

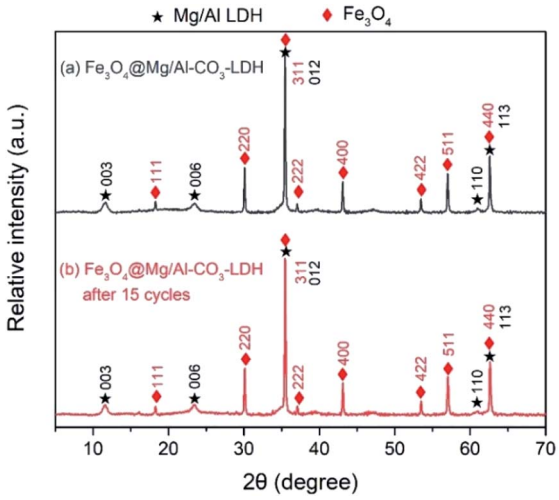


Fig. 4 XRD patterns of $Fe_3O_4$@Mg/Al-$CO_3$-LDH magnetic nano-adsorbent before and after 15 cycles of $PO_4^{3-}$-adsorption and regeneration.

$Fe_3O_4$@Mg/Al-$CO_3$-LDH magnetic nano-adsorbent can still maintain its structural stability, and thus has important potential for recycling.[58]

To explore the adsorption and desorption of $PO_4^{3-}$, the FTIR spectra of $Fe_3O_4$@Mg/Al-$CO_3$-LDH were measured for the as-synthesized, $PO_4^{3-}$-adsorbed, and regenerated after 15 cycles of $PO_4^{3-}$-adsorption samples, as shown in Fig. 5(a)–(c), respectively. The Fe–O vibration peak[59] appeared at 586 $cm^{-1}$ before and after adsorption and desorption, showing the stable assembly between $Fe_3O_4$ and Mg/Al-$CO_3$-LDH.

As shown in Fig. 5(a), the spectrum of the as-synthesized sample exhibits peaks at 448 $cm^{-1}$, 681 $cm^{-1}$, and 788 $cm^{-1}$, which are attributed to the vibration of Mg–OH,[60] Mg–O–Al,[61] and Al–OH,[60] respectively. The two peaks located at 3445 $cm^{-1}$ and 1637 $cm^{-1}$ are related to the stretching and bending modes of the water molecule existing in the interlayer structure, respectively.[62] These peaks indicate the successful synthesis of the layered structure Mg/Al-LDH. As the interlayer anion, the vibration of $CO_3^{2-}$ appears[35] at 1362 $cm^{-1}$ and 1502 $cm^{-1}$. During the hydrothermal process, urea decomposes at high temperature and produces the $CO_3^{2-}$ anion,[63] which then enters Mg/Al-LDH to form the interlayer anion. Moreover, there is a small peak located at 1385 $cm^{-1}$, corresponding to the $NO_3^-$ vibration, but it is rather weak. This is due to the use of nitrate during the synthetic process, where a small amount of $NO_3^-$ existing in $Fe_3O_4$@Mg/Al-$CO_3$-LDH was not replaced by $CO_3^{2-}$.

As shown in Fig. 5(b), in the spectrum of the $PO_4^{3-}$-adsorbed sample, the Fe–O vibration and the stretching and bending modes of the water molecule remained, but the vibrations resulting from Mg–OH, Mg–O–Al, and Al–OH almost disappear. Especially, there is no $CO_3^{2-}$ vibration at 1502 $cm^{-1}$, and only a very weak $CO_3^{2-}$ peak at 1362 $cm^{-1}$. On the other hand, new peaks at 2484 $cm^{-1}$, 2401 $cm^{-1}$, 1088 $cm^{-1}$, and 901 $cm^{-1}$ appear, which are due to the vibrations of $PO_4^{3-}$.[25,64,65] These results clearly indicate that the anion exchange[26] really occurred for $Fe_3O_4$@Mg/Al-$CO_3$-LDH after adsorbing $PO_4^{3-}$, which is the process to use $PO_4^{3-}$ to replace $CO_3^{2-}$. It is most probably the first mechanism for the synthesized $Fe_3O_4$@Mg/Al-$CO_3$-LDH to adsorb $PO_4^{3-}$ in solution. Due to the disappearance of the vibrations of Mg–OH and Al–OH, it means that they can be protonated and become positively charged, and thus they can adsorb the negatively charged $PO_4^{3-}$ due to electrostatic adsorption on the surface of LDH.[29] This may be the second mechanism to adsorb $PO_4^{3-}$ in solution. The disappearance of the vibration of Mg–O–Al may be possibly explained by the fact that, as a ligand anion,[29] $PO_4^{3-}$ can be complexed with the $Al^{3+}$ cation on the surface of $Fe_3O_4$@Mg/Al-$CO_3$-LDH. This ligand exchange may be the third mechanism to adsorb $PO_4^{3-}$ in solution. The ability to perform these three mechanisms for the synthesized $Fe_3O_4$@Mg/Al-$CO_3$-LDH is consistent with the reported $PO_4^{3-}$-adsorbed LDHs.[26,29,33]

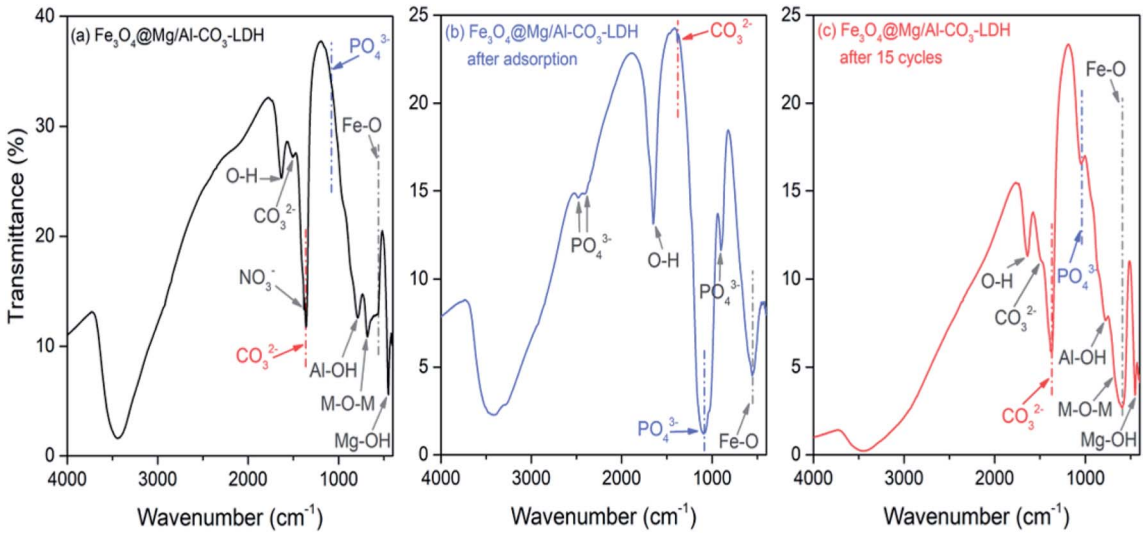


Fig. 5 FTIR spectra of $Fe_3O_4$@Mg/Al-$CO_3$-LDH magnetic nano-adsorbents. (a) As-prepared, (b) $PO_4^{3-}$-adsorbed, and (c) regenerated after 15 cycles of $PO_4^{3-}$-adsorption.

As shown in Fig. 5(c), in the spectrum of the regenerated sample after 15 cycles of $PO_4^{3-}$-adsorption, the positions and intensities of the FTIR peaks are almost the same as that in Fig. 4(a) of the as-synthesized sample. This means that the desorption was successful, and the regenerated $Fe_3O_4$@Mg/Al-$CO_3$-LDH returned to its original state with a strong ability to be recycled. It should be noted that there is still a weaker peak at 1088 $cm^{-1}$ due to $PO_4^{3-}$, which indicates a small amount of was $PO_4^{3-}$ left in $Fe_3O_4$@Mg/Al-$CO_3$-LDH after 15 cycles. However, it had no great effect on the phosphate adsorption capacity, as stated in Section 3.3, since most of the interlayer anions were exchanged by $CO_3^{2-}$ during the desorption process.

It was reported[52] that for MgAl-LDO calcined at 500 °C for 4 h after its synthesis, the FTIR band of –OH was shifted to a higher frequency from 1644 $cm^{-1}$ to 1664 $cm^{-1}$ after $F^-$ adsorption, which may be due to the adsorption of $F^-$. However, as can be seen in Fig. 5(a)–(c), the band due to OH appears at 1637 $cm^{-1}$, 1640 $cm^{-1}$, and 1638 $cm^{-1}$ for the as-synthesized, $PO_4^{3-}$-adsorbed, and regenerated $Fe_3O_4$@Mg/Al-$CO_3$-LDH samples, respectively. Thus, the absence of a shift in the OH band means that the synthesized $Fe_3O_4$@Mg/Al-$CO_3$-LDH did not adsorb $F^-$. This is in good agreement with the determination results by ion chromatography, indicating there was no change for the trace concentrations of $F^-$ and $Cl^-$ before and after adsorption (see Fig. 8 and 9 in Section 3.2, respectively). According to the literature, phosphate adsorption by some non-LDH adsorbents[66–70] and some LDH adsorbents[23–26,31,33] is greatly affected by $F^-$ or $Cl^-$ due to their adsorption. For LDHs, considering the bonding strength between the layers and interlayer anions in aqueous solution,[17] the strength of phosphates is generally higher than that of $F^-$ and $Cl^-$. Since there is a large amount of phosphate in aqueous solution, the adsorption possibility of phosphate is higher than that of $F^-$ or $Cl^-$. However, it is still inevitable that a small amount of $F^-$ and $Cl^-$ will be adsorbed,[23–26,31,33] although this possibility is small. Thus, to further decrease this possibility, for the synthesized nano-adsorbent of $Fe_3O_4$@Mg/Al-$CO_3$-LDH, $CO_3^{2-}$ was employed as the interlayer anion. The bonding strength of $CO_3^{2-}$ is the highest,[17] much greater than that of $F^-$ and $Cl^-$. During the phosphate adsorption process, a lot of $CO_3^{2-}$ anions will be exchanged in the solution, which will further inhibit the adsorption of trace $F^-$ and $Cl^-$ anions. Moreover, if some $OH^-$ anions exist in solution, the adsorption efficiencies[19] will further decline due to the combined effects of increasing competition from the $OH^-$ anion and the Coulomb repulsion between the negative-charged surface of the LDH adsorbent and $F^-$ or $Cl^-$. If there is insufficient positive charge such as $H^+$ on the surface of the LDH adsorbent, and there are enough anions such as $CO_3^{2-}$ and $PO_4^{3-}$, which have a much higher bonding strength than $F^-$ and $Cl^-$, to strongly compete with $F^-$ and $Cl^-$ anions, the synthesized magnetic nano-adsorbent $Fe_3O_4$@Mg/Al-$CO_3$-LDH should not adsorb $F^-$ and $Cl^-$ anions.

Fig. 6 shows the magnetic hysteresis loops of $Fe_3O_4$, and $Fe_3O_4$@Mg/Al-$CO_3$-LDH before and after 15 cycles of $PO_4^{3-}$-adsorption. Compared with the magnetic saturation value of 102 emu $g^{-1}$ for the pure $Fe_3O_4$ nanoparticles, that for the as-synthesized $Fe_3O_4$@Mg/Al-$CO_3$-LDH drops to 36.75 emu $g^{-1}$ since the non-magnetic Mg/Al-$CO_3$-LDH shields the magnetic $Fe_3O_4$. Even if after 15 cycles, it was still 36.47 emu $g^{-1}$. This value is sufficient to achieve repeated rapid magnetic extraction and separation. More importantly, it should be noted that the two loop curves before and after $PO_4^{3-}$-adsorption come close to coinciding in shape. This truthfully reflects that the thickness of the Mg/Al-$CO_3$-LDH coating layer did not change, which indicates almost no etching and degradation occurred even after 15 cycles of adsorption, separation and desorption. Based on this, the structural stability indicated by the above Fig. 4(b), which is also the result after 15 cycles of $PO_4^{3-}$-adsorption, means that the two-dimensional crystalline nanostructure of Mg/Al-$CO_3$-LDH and the interlayer anion $CO_3^{2-}$ in the layered double hydroxide were both maintained rather stably. Actually, it can be seen in Fig. 5(c) that after 15 cycles of adsorption, separation and desorption, the FTIR peak intensity of $CO_3^{2-}$ is as strong as that of the as-synthesized $Fe_3O_4$@Mg/Al-$CO_3$-LDH, as seen in Fig. 5(a). This means that the content of $CO_3^{2-}$ was almost fully recovered even after 15 cycles of $PO_4^{3-}$-desorption, which can provide an excellent performance for stable dephosphorization.

Fig. 7(a) and (b) show the $N_2$ adsorption–desorption isotherms and BJH (Barrett–Joyner–Halenda) pore diameter distribution curves of $Fe_3O_4$@Mg/Al-$CO_3$-LDH, respectively. In Fig. 7(a), there is a clear hysteresis loop at a high relative pressure of $P/P_0 > 0.6$, which is a typical type IV adsorption isotherm[28] according to the IUPAC classification. When $P/P_0 > 0.9$, there is no saturated adsorption platform, and rapid adsorption and desorption occur in this high pressure region. This indicates that the loop can be further classified as type H3,[28] which means the pores in $Fe_3O_4$@Mg/Al-$CO_3$-LDH are mainly mesoporous. This was verified by Fig. 7(b), where the pore size distribution is mainly in the range of 5–50 nm, with an average size of 15.1 nm and total pore volume of 0.59 $cm^3$ $g^{-1}$. The formation of these mesoporous pores in $Fe_3O_4$@Mg/Al-$CO_3$-LDH is related to the slit-shaped pores or voids created within the aggregates of platy particles.[28,71] Generally, the

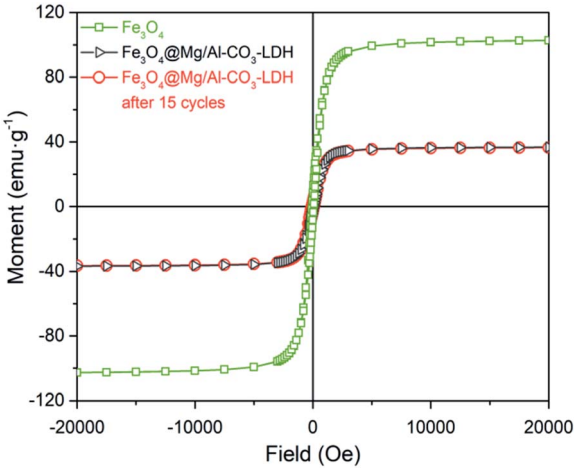


Fig. 6 Magnetic hysteresis loop analysis for $Fe_3O_4$ nanoparticle, and prepared $Fe_3O_4$@Mg/Al-$CO_3$-LDH magnetic nano-adsorbent before and after 15 cycles of $PO_4^{3-}$-adsorption and regeneration.

 

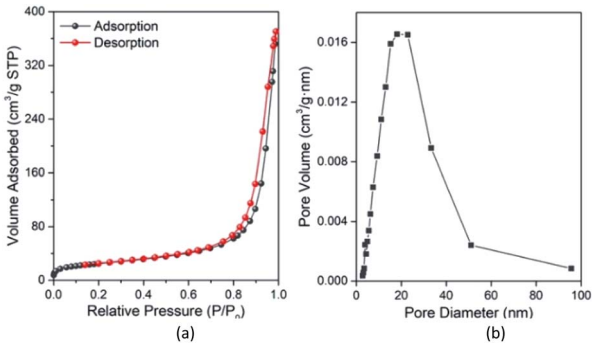


Fig. 7 $N_2$ adsorption–desorption isotherms (a) and Barrett–Joyner–Halenda (BJH) pore diameter distribution curve (b) of the prepared $Fe_3O_4$@Mg/Al-$CO_3$-LDH magnetic nano-adsorbent.

specific surface area and total pore volume will affect the chance of contact between the adsorbent and the adsorbate, thereby affecting the adsorption effect of the adsorbent.[28,72] According to the BET (Brunauer–Emmett–Teller) method,[73] the specific surface area of $Fe_3O_4$@Mg/Al-$CO_3$-LDH was calculated to be 88.4 $m^2\ g^{-1}$. Thus, the hydrothermally synthesized $Fe_3O_4$@Mg/Al-$CO_3$-LDH can adsorb $PO_4^{3-}$ in solution rapidly and efficiently.

### 3.2 Optimized pretreatment by $Fe_3O_4$@Mg/Al-$CO_3$-LDH

For 80 mL solution containing 1.00 mg $L^{-1}$ $F^-$, 1.00 mg $L^{-1}$ $Cl^-$ and 100 mg P per L $PO_4^{3-}$ are the optimized adsorbent amount and adsorption time for $Fe_3O_4$@Mg/Al-$CO_3$-LDH, respectively. These optimized pretreatment conditions were utilized for the analysis of real samples, as stated in Section 4.

By using different amounts of $Fe_3O_4$@Mg/Al-$CO_3$-LDH magnetic nano-adsorbent to adsorb $PO_4^{3-}$ for the same adsorption time of 60 min, Fig. 8 shows the chromatograms, in which three chromatographic peaks at about 3 min, 7 min, 22 min correspond to $F^-$, $Cl^-$, and $PO_4^{3-}$, respectively. Their concentrations were calculated based on their peak area, and plotted at the top of Fig. 8. With the addition of $Fe_3O_4$@Mg/Al-$CO_3$-LDH in the solution, the concentration of both $F^-$ and $Cl^-$ was always maintained at around 1.00 mg $L^{-1}$ with the fluctuation of ±2%, as shown in the top-left and top-middle of Fig. 8. This indicates that $Fe_3O_4$@Mg/Al-$CO_3$-LDH will not adsorb any $F^-$ and $Cl^-$ anions in the solution regardless of the adsorbent amount used, which is the most important factor to determine trace $F^-$ and $Cl^-$ in solution. On the other hand, only a small amount of the nano-adsorbent, such as 20 and 50 mg, could make the residual $PO_4^{3-}$ concentration decrease greatly from 100 mg P per L to 64.5 and 49.5 mg P per L, respectively, as shown in the top-right of Fig. 8. However, when the absorbent amount was further increased to 80 mg, the residual $PO_4^{3-}$ concentration did not further decrease since equilibrium between $PO_4^{3-}$ and $CO_3^{2-}$ was reached. Thus, the optimized adsorbent amount of 50 mg $Fe_3O_4$@Mg/Al-$CO_3$-LDH is enough for 80 mL solution with 100 mg P per L $PO_4^{3-}$.

By using 50 mg $Fe_3O_4$@Mg/Al-$CO_3$-LDH to adsorb $PO_4^{3-}$ in 80 mL solution for different times, the residual concentration of

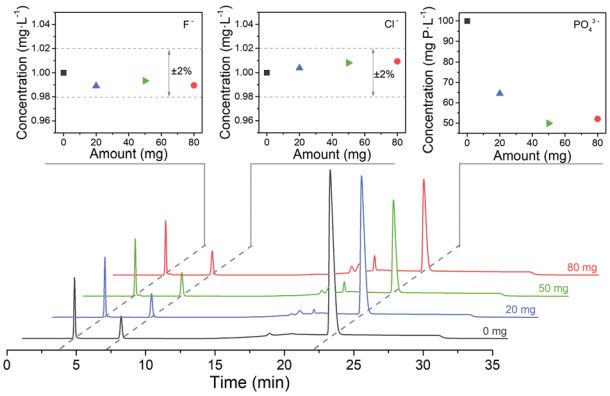


Fig. 8 Chromatograms for the solution with 1.00 mg $L^{-1}$ $F^-$, 1.00 mg $L^{-1}$ $Cl^-$ and 100 mg P per L $PO_4^{3-}$ using 0, 20, 50, and 80 mg $Fe_3O_4$@Mg/Al-$CO_3$-LDH magnetic nano-adsorbent, respectively. The same adsorption time of 60 min was applied.

$PO_4^{3-}$ and $F^-$ and $Cl^-$ anions in the solution was determined by chromatography, as plotted in Fig. 9. According to Fig. 9(a), the concentration of both $F^-$ and $Cl^-$ was maintained at around 1.00 mg $L^{-1}$ with the fluctuation of ±2%, regardless of the adsorbent time used. Similarly, as indicated in the plots at the top of Fig. 8, $Fe_3O_4$@Mg/Al-$CO_3$-LDH did not adsorb any $F^-$ and $Cl^-$ anions in the solution, no matter how long the interaction time. However, for $PO_4^{3-}$, even with fast magnetic separation immediately after the addition of $Fe_3O_4$@Mg/Al-$CO_3$-LDH in the solution, the residual $PO_4^{3-}$ concentration directly declined to 72.9 mg P per L. Also, after 2 and 5 min adsorption, it decreased to 60.3 and 52.2 mg P per L, respectively. With a further increase in the adsorption time, the adsorption of $PO_4^{3-}$ slows down to the equilibrium stage, until the residual $PO_4^{3-}$ concentration finally reached 48.1 mg P per L after 120 min adsorption. According to the formula for phosphate adsorption capacity,[74] as stated in Section 2.3, the capacity of $Fe_3O_4$@Mg/Al-$CO_3$-LDH is 83.04 mg P per g for 120 min adsorption. Even for 5 min adsorption, it is still as high as 76.48 mg P per g. Thus, the optimized adsorption time was chosen to be 5–60 min for the solution using 50 mg $Fe_3O_4$@Mg/Al-$CO_3$-LDH.

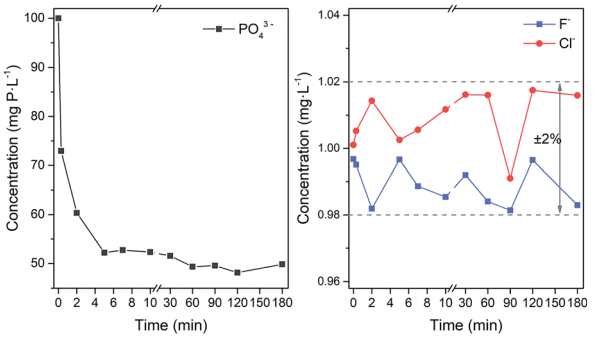


Fig. 9 Determined concentrations by chromatography for 80 mL solution with 1.00 mg $L^{-1}$ $F^-$, 1.00 mg $L^{-1}$ $Cl^-$ and 100 mg P per L with the adsorption time. In the adsorption experiment, the used $Fe_3O_4$@Mg/Al-$CO_3$-LDH magnetic nano-adsorbent is 50 mg.

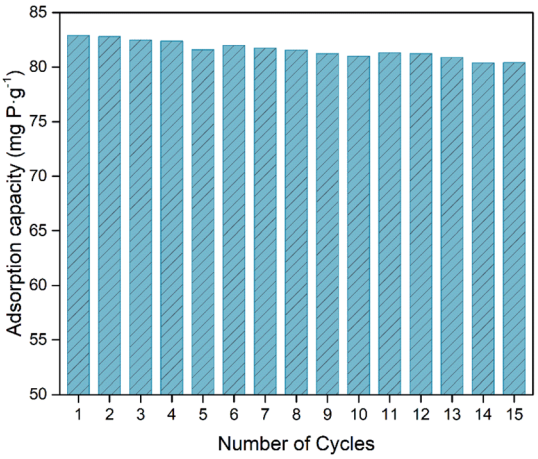


Fig. 10 Phosphate adsorption capacities of $Fe_3O_4$@Mg/Al-$CO_3$-LDH magnetic nano-adsorbent for 15 cycles of $PO_4^{3-}$-adsorption–desorption, respectively. For each cycle, 80 mL solution with 1.00 mg $L^{-1}$ $F^-$, 1.00 mg $L^{-1}$ $Cl^-$ and 100 mg P per L is adsorbed by 50 mg $Fe_3O_4$@Mg/Al-$CO_3$-LDH magnetic nano-adsorbent for 60 min. The desorption solution is 15 mL mixture of 5 wt% NaOH and 10 wt% $Na_2CO_3$ and the desorption time is 30 min.

### 3.3 Recyclability of $Fe_3O_4$@Mg/Al-$CO_3$-LDH

The recyclability of an adsorbent is vital for its practical application,[31,58] and the premise for recycling is the stability of its structure. The crystalline structure stability, the adsorption stability, and the coating layer stability of $Fe_3O_4$@Mg/Al-$CO_3$-LDH after 15 cycles of $PO_4^{3-}$-adsorption and regeneration were confirmed by XRD, as shown in Fig. 4(b), FTIR, as shown in Fig. 5(c), and magnetic hysteresis loop analysis, as shown in Fig. 6, respectively.

To evaluate the recyclability of the $Fe_3O_4$@Mg/Al-$CO_3$-LDH magnetic nano-adsorbent, the phosphate adsorption capacities were determined for each cycle and shown in Fig. 10, where the 60 min adsorption, 30 min desorption and regeneration processes are stated in Section 2.3. The initial capacity of 83.04 mg P per g calculated from Fig. 9 was used for the as-synthesized $Fe_3O_4$@Mg/Al-$CO_3$-LDH. For the subsequent cycles, the phosphate adsorption capacity decreased but very slowly. Even after 15 desorption–adsorption cycles, the capacity was still as high as 80.41 mg P per g, which is only 3.2% lower than the initial 83.04 mg P per g. Among the 15 cycles, the maximum decrease occurred in the 5th cycle, but not more than 1%, and the average decrease was as low as ~0.2%. This clearly indicates that the synthesized $Fe_3O_4$@Mg/Al-$CO_3$-LDH has excellent recyclability and stability, maintaining high phosphate adsorption capacities even after manifold cycles.

Table 1 presents the phosphate adsorption capacity, adsorption time, and recycle number of various magnetic adsorbents. These adsorbents, LDH adsorbents with interlayer anion and non-LDH adsorbents, can all be used to efficiently adsorb $PO_4^{3-}$ in solution. Compared with most of the adsorbents, the phosphate capacity per unit mass of the synthesized $Fe_3O_4$@Mg/Al-$CO_3$-LDH is as high as 76.48 mg P per g, higher than 1.8675–36.9 mg P per g, but somewhat lower[25,31,69,74] than 128–252.88 mg P per g of these four adsorbents. However, they used about 360–4320 min to adsorb phosphates in solution. It

Table 1 Comparison of the adsorption time, adsorption capacity and the number of reuse cycles by various magnetic adsorbents for the adsorption of the $PO_4^{3-}$ phosphate group

| Adsorbent | Interlayer anion for LDH[g] | Adsorption time (min) | Adsorption capacity[a] (mg P per g) | Cycle no. | Ref. |
|---|---|---|---|---|---|
| ZnFeZr adsorbent@$Fe_3O_4$/$SiO_2$ | $Cl^-$ | 60 | | 20 | 23 |
| Magnetic Fe/Mn oxide composites (TS-N) | $Cl^-$ | 90 | 26.0 | | 24 |
| $Fe_3O_4$/Zn–Al–Fe–La-LDH | $Cl^-$ and $SO_4^{2-}$ | 1440 | 169.5 | 4[b] | 25 |
| $Fe_3O_4$@Zn–Al-LDH | $CO_3^{2-}$ | 60 | 36.9 | | 26 |
| $Fe_3O_4$@Mg–Al-LDH | | | 31.7 | | |
| $Fe_3O_4$@Ni–Al-LDH | | | 26.5 | | |
| Fe/$CaCO_3$_PVA | Non-LDH | | 16.7 | | 75 |
| Fe/$MgCO_3$_PVA | | | 16.3 | | |
| $Fe_3O_4$@$SiO_2$–$CeO_2$ | Non-LDH | 1440 | 10.8 | 2[c] | 76 |
| Ce–Ti@ $Fe_3O_4$ | Non-LDH | 1440 | 11.10 | | 66 |
| Carboxylated chitosan–$Fe_3O_4$ | Non-LDH | 60 | 1.8675 | | 67 |
| La–chitosan magnetic spheres | Non-LDH | 300 | 27.78 | | 68 |
| $ZrO_2$/$Fe_3O_4$ | Non-LDH | 1440 | 29.5 | | 77 |
| Magnetic *Caragana korshinskii* biochar/Mg–Al-LDH | $Cl^-$ | 720 | 252.88 | 5[d] | 31 |
| $Fe_3O_4$@alkali-treated calcium-silicate | Non-LDH | 4320 | 128 | 2[e] | 69 |
| $Fe_3O_4$@gelatin encapsulated hydrotalcite | $CO_3^{2-}$ | 40 | 32.73 | 4[f] | 33 |
| NrGO/$Fe_3O_4$ | Non-LDH | 360 | 135.3 | 5 | 74 |
| Humic acid coated magnetite nanoparticles | Non-LDH | 180 | 28.9 | | 70 |
| $Fe_3O_4$@Mg/Al-$CO_3$-LDH | $CO_3^{2-}$ | 5 | 76.48 | 15 | This work |

[a] Adsorption capacity of phosphate, $Q_e = (C_0 - C_e)V/m$, where $C_0$ and $C_e$ are the initial and equilibrium phosphate concentration in mg $L^{-1}$, $V$ is the volume of phosphate solution in L, and $m$ is the dry weight of the adsorbent in g. [b] The adsorption capacity decreased to 31 mg $g^{-1}$ after 4 cycles. [c] The adsorption capacity decreased to 25.71 mg $g^{-1}$ after 5 cycles. [d] The adsorption efficiency was reduced to 70.01% after 4 cycles. [e] The adsorption capacity decreased to 4.8 mg $g^{-1}$ after 2 cycles. [f] The adsorption capacity decreased to 20.2 mg $g^{-1}$ after 2 cycles. [g] The information is summarized from the description of preparation processes, or FTIR, XPS and other characterization in refs.

 

should be noted that the capacity is related to the adsorption time used. Even if the adsorption time used is as fast as 5 min, which is 1/8–1/288 of the reported times listed in Table 1, the adsorption capacity of 76.48 mg P per g for $Fe_3O_4$@Mg/Al-$CO_3$-LDH is high enough to adsorb $PO_4^{3-}$ rapidly and efficiently so as to determine $F^-$ and $Cl^-$ without serious interference due to $PO_4^{3-}$. In the case of the recycle number, which is one of the vital properties for the recyclability of an adsorbent, it is 15 cycles for $Fe_3O_4$@Mg/Al-$CO_3$-LDH, more than the reported 2–5 cycles. The reported recycle number could reach up to 20 cycles,[23] but there was no information about the phosphate adsorption capacity. According to Table 1, if only considering magnetic LDHs with a $CO_3^{2-}$ interlayer anion, $Fe_3O_4$@Mg/Al-$CO_3$-LDH behaves very well to adsorb $PO_4^{3-}$ in solution, with four times greater cycle number and two times greater phosphate adsorption capacity.

## 4 Analysis of real samples

Phosphate and fluorophosphate laser glasses contain high $PO_4^{3-}$ and a certain amount of various monovalent, divalent, trivalent metal cations. The leaching solutions from these glasses were determined before and after adsorption pretreatment using the $Fe_3O_4$@Mg/Al-$CO_3$-LDH magnetic nano-adsorbent, and the chromatograms are shown in Fig. 11. As seen in Fig. 11(a) for the phosphate ($P_2O_5$ molar ratio of both N31 and N41 glasses is close to 60%) with high $PO_4^{3-}$ but low $F^-$ and $Cl^-$, the strong peak at 22.36 min due to $PO_4^{3-}$ is too overloaded, and thus it seems to be a leading peak with 100 μS conductivity. After the adsorption pretreatment, the 22.36 min peak shape became normal and its intensity decreased greatly to 10 μS. This indicates that $Fe_3O_4$@Mg/Al-$CO_3$-LDH could efficiently adsorb $PO_4^{3-}$ in the multi-ion leaching solution in a short time of only 5 min. On the other hand, $Fe_3O_4$@Mg/Al-$CO_3$-LDH did not adsorb any $F^-$ or $Cl^-$. The peaks at 3.79 and 7.34 min are due to $F^-$ and $Cl^-$, respectively, and their intensities did not change after the adsorption pretreatment. As seen in Fig. 11(b) for the fluorophosphate with a high $F^-$ and $PO_4^{3-}$ content but low $Cl^-$, the 22.36 min $PO_4^{3-}$ peak almost disappeared after the adsorption pretreatment by $Fe_3O_4$@Mg/Al-$CO_3$-LDH for 5 min. The strong $F^-$ peak at 3.79 min and the weak $Cl^-$ peak at 7.34 min did not change after the pretreatment. Regardless of a high or low $PO_4^{3-}$ content in a multi-ion solution, the synthesized $Fe_3O_4$@Mg/Al-$CO_3$-LDH magnetic nano-adsorbent can adsorb and extract $PO_4^{3-}$ rapidly. Also, regardless of a high or low $F^-$ or $Cl^-$ content in a multi-ion solution, the addition and extraction of the nano-adsorbent did not result in any change in the contents of $F^-$ or $Cl^-$. These two facts determine the usefulness of the nano-adsorbent for specific applications, *i.e.* the removal of $PO_4^{3-}$, and especially the determination of $F^-$/$Cl^-$ after removing $PO_4^{3-}$ in a multi-ion solution. By using the $Fe_3O_4$@Mg/Al-$CO_3$-LDH adsorption pretreatment, the pretreated solution can be utilized for other determination techniques or methods since there will be no serious interference from $PO_4^{3-}$ in the solution. Considering chromatography, the determination time for the accurate determination of $F^-$ and $Cl^-$ can be greatly shortened after removing $PO_4^{3-}$. More importantly, without being affected by $PO_4^{3-}$ and fully retaining trace $F^-$ and $Cl^-$, a continuous analysis or on-line test can be done during processes in the laboratory and industry in fields such as pharmaceuticals and biomaterials. If $PO_4^{3-}$ is not removed from a $PO_4^{3-}$-rich solution, the next injection must not be allowed.[11]

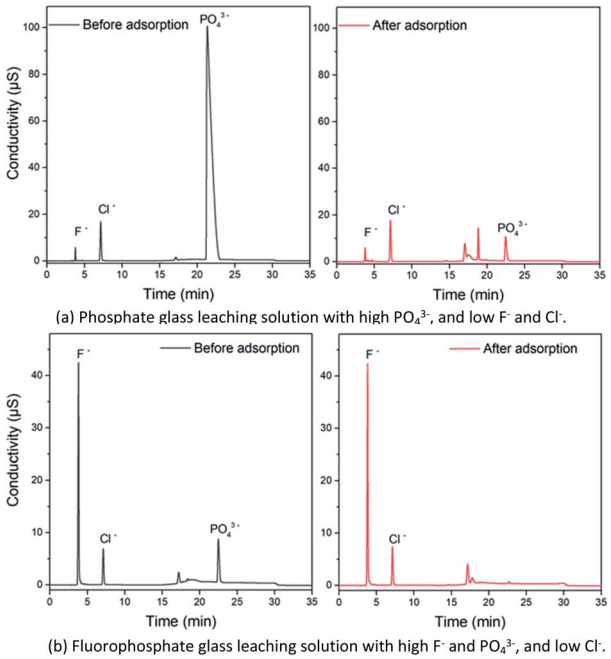


Fig. 11 Chromatograms for the leaching solutions of phosphate glass (a) and fluorophosphate glass (b) before and after 5 min adsorption by 50 mg $Fe_3O_4$@Mg/Al-$CO_3$-LDH magnetic nano-adsorbent.

By chromatography, Table 2 lists the determined results of $F^-$ and $Cl^-$ for various real samples, such as a certified reference ore material (GBW07108 containing F, Cl and P, as well as 66 other elements), silicate glass, fluorophosphate glass, phosphate laser glasses, and environmental water samples. Specifically, 80 mL sample solution was pretreated using $Fe_3O_4$@Mg/Al-$CO_3$-LDH under the optimized conditions. For the certified ore sample, the determined values of 0.395 and 0.0071 mg $L^{-1}$ are very close to the certified values of 0.406 and 0.0078 mg $L^{-1}$ for $F^-$ and $Cl^-$, respectively. After determining $F^-$ and $Cl^-$ for the other samples, a certain amount of $F^-$ and $Cl^-$ standard solutions was added, *i.e.* the added content was 1.00 mg $L^{-1}$. Subsequently, the contents of $F^-$ and $Cl^-$ in the solution re-pretreated by $Fe_3O_4$@Mg/Al-$CO_3$-LDH were measured again. Accordingly, the spiked recoveries were calculated. As seen in Table 2, these spiked recoveries were all within an acceptable range of 95.7–104.9%. Thus, the above determinations prove the accuracy to determine $F^-$ and $Cl^-$ in multi-ion solutions pretreated by the synthesized $Fe_3O_4$@Mg/Al-$CO_3$-LDH magnetic nano-adsorbent.

It should be noted that the pH values of real sample solutions may vary from sample to sample, especially when dissolving solid samples by acid or alkali. The pH value of the solution will affect the existing form of phosphate anions,[17,26,29] such as $PO_4^{3-}$, $HPO_4^{2-}$ and $H_2PO_4^-$. Thus, two phosphate

Table 2 Determination of $F^-$ and $Cl^-$ anions in a certified reference ore sample, silicate glasses, fluorophosphate glasses, phosphate glasses and river water samples by ion chromatography after adsorption pretreatment by $Fe_3O_4$@Mg/Al-$CO_3$-LDH

| | $F^-$ | | | $Cl^-$ | | |
|---|---|---|---|---|---|---|
| Sample | Added (mg $L^{-1}$) | Found (mg $L^{-1}$) | Recovery (%) | Added (mg $L^{-1}$) | Found (mg $L^{-1}$) | Recovery (%) |
| GBW07108[a] | 0.406[b] | 0.395 | 97.3 | 0.078[b] | 0.071 | 91.0 |
| | 1.00 | 1.444 | 104.9 | 1.00 | 1.092 | 102.1 |
| Silicate glass | 0 | 9.970 | — | 0 | 0.083 | — |
| | 1.00 | 10.927 | 95.7 | 1.00 | 1.069 | 98.6 |
| Fluorophosphate glass | 0 | 21.972 | — | 0 | 0.066 | — |
| | 1.00 | 23.012 | 104.0 | 1.00 | 1.060 | 99.4 |
| N31 phosphate glass, pot melting | 0 | 0.744 | — | 0 | 0.251 | — |
| | 1.00 | 1.738 | 99.4 | 1.00 | 1.245 | 99.4 |
| N41 phosphate glass, pot melting | 0 | 0.814 | — | 0 | 0.585 | — |
| | 1.00 | 1.800 | 98.6 | 1.00 | 1.558 | 97.3 |
| N41 phosphate glass, continuous | 0 | 1.267 | — | 0 | 0.459 | — |
| melting | 1.00 | 2.277 | 101.0 | 1.00 | 1.501 | 104.2 |
| River water | 0 | 0.153 | — | 0 | 7.351 | — |
| | 1.00 | 1.150 | 99.7 | 1.00 | 8.338 | 98.7 |

[a] The certified reference ore samples were approved by the General Administration of Quality Supervision, Inspection and Quarantine of the People's Republic of China, which were mainly composed of silicate, carbonate and oxide of Al, Fe, Mg and Ca. [b] The certified content of $F^-$ and $Cl^-$ in the certified reference material GBW07108.

solutions were obtained by dissolving high purity $Na_3PO_4$ or $NaH_2PO_4$ in deionized water without adding any acid and alkali, and treated with the magnetic nano-adsorbent of $Fe_3O_4$@Mg/Al-$CO_3$-LDH, and their ion chromatogram peaks due to phosphate greatly decreased. The large decrease indicates the effective adsorption of both $Na_3PO_4$ and $NaH_2PO_4$ solutions. This implies that no matter the existing form of phosphate anions, such as $PO_4^{3-}$ and $H_2PO_4^-$, the synthesized $Fe_3O_4$@Mg/Al-$CO_3$-LDH can adsorb them efficiently. On the other hand, the pH value of real sample solutions as in the above applications is not adjusted by acid and alkali to avoid any further disturbance in the trace determination of $F^-$ and $Cl^-$ by ion chromatography.

## 5 Conclusion

Using the urea hydrothermal method, the layered double hydroxide Mg/Al-$CO_3$-LDH was synthesized and aggregated as small crystal plates on $Fe_3O_4$ nanoparticles, which retained its original crystalline state with high magnetism. The magnetic saturation value of 36.47 emu $g^{-1}$ was sufficient to achieve rapid magnetic extraction–separation during $PO_4^{3-}$-adsorption by $Fe_3O_4$@Mg/Al-$CO_3$-LDH. As a recyclable magnetic nano-adsorbent, its structural stability was confirmed after 15 regeneration cycles for $PO_4^{3-}$-adsorption and desorption. The vibrations of the $CO_3^{2-}$ and $PO_4^{3-}$ groups, and the Mg–OH, Al–OH, and Mg–O–Al bonds indicated that the mechanism for the adsorption of $PO_4^{3-}$ by $Fe_3O_4$@Mg/Al-$CO_3$-LDH is related to the anion exchange between the interlayer anion $CO_3^{2-}$ and $PO_4^{3-}$ in solution, the LDH surface electrostatic adsorption for $PO_4^{3-}$ in solution, and the ligand exchange between LDH and $PO_4^{3-}$ in solution. Since mesoporous pores are created within the aggregates of small crystal plates during the synthesis of $Fe_3O_4$@Mg/Al-$CO_3$-LDH, its large specific surface area and total pore volume are 88.4 $m^2$ $g^{-1}$ and 0.59 $cm^3$ $g^{-1}$, respectively. These endow the magnetic nano-adsorbent with a high phosphate adsorption capacity of 83.04 mg P per g for 120 min adsorption, or still up to 76.48 mg P per g for rapid 5 min adsorption. Even after 15 desorption–adsorption cycles, the capacity was still as high as 80.41 mg P per g with only a decline by 3.2%. Compared with other magnetic LDHs with $CO_3^{2-}$, the synthesized $Fe_3O_4$@Mg/Al-$CO_3$-LDH exhibited very good ability to adsorb $PO_4^{3-}$, with four times greater cycle number, two times greater phosphate adsorption capacity, and eight-twelve times less adsorption time. More importantly, regardless of a high or low $F^-$ or $Cl^-$ content, and regardless of the used amount and adsorption time of $Fe_3O_4$@Mg/Al-$CO_3$-LDH, the addition and extraction of the nano-adsorbent did not result in any change in the contents of $F^-$ and $Cl^-$ in a multi-ion solution. Thus, the usefulness of the synthesized $Fe_3O_4$@Mg/Al-$CO_3$-LDH is concentrated on two specific applications, the removal of $PO_4^{3-}$, and especially the accurate determination of $F^-$ and $Cl^-$ after the removal of $PO_4^{3-}$. By optimizing the nano-adsorbent amount and adsorption time, $Fe_3O_4$@Mg/Al-$CO_3$-LDH was successfully utilized to adsorb $PO_4^{3-}$ rapidly and determine $F^-$/$Cl^-$ accurately by ion chromatography for real samples such as certified reference ore materials, phosphate laser glass, fluorophosphate glass, silicate glass and environmental water samples. Currently, these applications are greatly beneficial for product quality monitoring for extremely hazardous $F^-$ and $Cl^-$ to protect the ecological environment. On the other hand, excess P will lead to widespread eutrophication in aquatic environments, in which algal blooms are also harmful towards human health due to cyanotoxins.[78] With the further development and progress on the adsorption capacity, adsorption recovery velocity, and adsorption kinetics,[78,79] studies will be devoted to online applications and widening the scope of these significant methods using LDH adsorbents, which will contribute immensely to environmental protection.

 

## Conflicts of interest

There are no conflicts to declare.

## Acknowledgements

The research work was financially supported by Nd-doped phosphate laser glass projects from National Major Science and Technology Project of China, National High Technology Research and Development Program for Inertial Confinement Fusion of China.

## References

1 F. Vasconcelos, S. Cristol, J. Paul, L. Montagne, F. Mauri and L. Delevoye, *Magn. Reson. Chem.*, 2010, **48**, S142–S150.
2 A. Salama, *Int. J. Biol. Macromol.*, 2019, **127**, 606–617.
3 H. Parham and N. Rahbar, *Talanta*, 2009, **80**, 664–669.
4 V. P. Kolotov and E. A. Arafa, *J. Radioanal. Nucl. Chem.*, 1993, **172**, 357–362.
5 P. Venkateswarlu, *Anal. Chim. Acta*, 1992, **262**, 33–40.
6 Z. Ni, Z. Rao and M. Li, *Anal. Chim. Acta*, 1996, **334**, 177–182.
7 P. Bermejo-Barrera, A. Moreda-Piñeiro and A. Bermejo-Barrera, *Spectrochim. Acta, Part B*, 2002, **57**, 327–337.
8 U. Nygren, H. Ramebäck, D. C. Baxter and C. Nilsson, *J. Anal. At. Spectrom.*, 2005, **20**, 529.
9 F. S. Stover, *J. Chromatogr. A*, 2002, **956**, 121–128.
10 L. E. Vanatta, D. E. Coleman and A. Woodruff, *J. Chromatogr. A*, 2003, **997**, 269–278.
11 E. Kaiser, J. S. Rohrer and K. Watanabe, *J. Chromatogr. A*, 1999, **850**, 167–176.
12 L. Al Attar, M. Al-Oudat, K. Shamali, B. A. Ghany and S. Kanakri, *Environ. Technol.*, 2012, **33**, 143–152.
13 W. Qiao, R. Liu, Z. Li, X. Luo, B. Huang, Q. Liu, Z. Chen, J. Tsoi, Y. X. Su, K. Cheung, J. P. Matinlinna, K. Yeung and Z. Chen, *Biomater. Sci.*, 2018, **6**, 2951–2964.
14 D. Štepec and M. Ponikvar-Svet, *Acta Chim. Slov.*, 2019, **66**, 255–275.
15 F. L. Theiss, G. A. Ayoko and R. L. Frost, *Appl. Surf. Sci.*, 2016, **383**, 200–213.
16 V. Rives and M. Angeles Ulibarri, *Coord. Chem. Rev.*, 1999, **181**, 61–120.
17 Q. Zhang, F. Ji, T. Zhao, Q. Shen, D. Fang, L. Kuang, L. Jiang and S. Ding, *Appl. Clay Sci.*, 2019, **174**, 159–169.
18 M. P. Bernardo and C. Ribeiro, *Mater. Res.*, 2018, **21**, e20171001.
19 F. Li, J. Jin, Z. Shen, H. Ji, M. Yang and Y. Yin, *J. Hazard. Mater.*, 2020, **388**, 121734.
20 C. V. Luengo, M. A. Volpe and M. J. Avena, *J. Environ. Chem. Eng.*, 2017, **5**, 4656–4662.
21 H. Hatami, A. Fotovat and A. Halajnia, *Appl. Clay Sci.*, 2018, **152**, 333–341.
22 S. M. Ashekuzzaman and J. Jiang, *Process Saf. Environ. Prot.*, 2017, **107**, 454–462.
23 A. Drenkova-Tuhtan, M. Schneider, M. Franzreb, C. Meyer, C. Gellermann, G. Sextl, K. Mandel and H. Steinmetz, *Water Res.*, 2017, **109**, 77–87.
24 C. Chon, D. Cho, I. Nam, J. Kim and H. Song, *J. Soils Sediments*, 2018, **18**, 946–956.
25 W. Qiao, H. Bai, T. Tang, J. Miao and Q. Yang, *Colloids Surf., A*, 2019, **577**, 118–128.
26 L. Yan, K. Yang, R. Shan, T. Yan, J. Wei, S. Yu, H. Yu and B. Du, *J. Colloid Interface Sci.*, 2015, **448**, 508–516.
27 R. Chitrakar, S. Tezuka, J. Hosokawa, Y. Makita, A. Sonoda, K. Ooi and T. Hirotsu, *J. Colloid Interface Sci.*, 2010, **349**, 314–320.
28 K. S. Triantafyllidis, E. N. Peleka, V. G. Komvokis and P. P. Mavros, *J. Colloid Interface Sci.*, 2010, **342**, 427–436.
29 F. Hu, M. Wang, X. Peng, F. Qiu, T. Zhang, H. Dai, Z. Liu and Z. Cao, *Colloids Surf., A*, 2018, **555**, 314–323.
30 J. Zhou, S. Yang, J. Yu and Z. Shu, *J. Hazard. Mater.*, 2011, **192**, 1114–1121.
31 Q. Cui, G. Jiao, J. Zheng, T. Wang, G. Wu and G. Li, *RSC Adv.*, 2019, **9**, 18641–18651.
32 B. Bekele, L. Lundehøj, N. D. Jensen, U. G. Nielsen and C. Forano, *Appl. Clay Sci.*, 2019, **176**, 49–57.
33 I. A. Kumar and N. Viswanathan, *J. Environ. Chem. Eng.*, 2018, **6**, 208–217.
34 M. Ogawa and H. Kaiho, *Langmuir*, 2002, **18**, 4240–4242.
35 F. Yang, S. Sun, X. Chen, Y. Chang, F. Zha and Z. Lei, *Appl. Clay Sci.*, 2016, **123**, 134–140.
36 M. M. Rao, B. R. Reddy, M. Jayalakshmi, V. S. Jaya and B. Sridhar, *Mater. Res. Bull.*, 2005, **40**, 347–359.
37 S. Ma, C. Fan, G. Huang, Y. Li, X. Yang and K. Ooi, *Eur. J. Inorg. Chem.*, 2010, **2010**, 2079–2083.
38 S. Li, Y. Shen, D. Liu, L. Fan, X. Zheng and J. Yang, *Compos. Interfaces*, 2012, **19**, 489–498.
39 J. Wang, D. Li, X. Yu, M. Zhang and X. Jing, *Colloid Polym. Sci.*, 2010, **288**, 1411–1418.
40 T. Hibino and H. Ohya, *Appl. Clay Sci.*, 2009, **45**, 123–132.
41 B. Li, J. He and D. G. Evans, *Chem. Eng. J.*, 2008, **144**, 124–137.
42 P. Zhang, T. Yamaguchi, B. N. Nair, K. Miyajima and G. M. Anilkumar, *RSC Adv.*, 2014, **4**, 41051–41058.
43 M. Yang, J. Liu, Z. Chang, G. R. Williams, D. O'Hare, X. Zheng, X. Sun and X. Duan, *J. Mater. Chem.*, 2011, **21**, 14741–14746.
44 S. Radha and A. Navrotsky, *J. Phys. Chem. C*, 2014, **118**, 29836–29844.
45 B. Li and J. He, *J. Phys. Chem. C*, 2008, **112**, 10909–10917.
46 G. K. Sarma and M. H. Rashid, *J. Chem. Eng. Data*, 2018, **63**, 2957–2965.
47 X. Lei, W. Lu, Q. Peng, H. Li, T. Chen, S. Xu and F. Zhang, *Appl. Catal., A*, 2011, **399**, 87–92.
48 X. Yuan, Y. Wang, J. Wang, C. Zhou, Q. Tang and X. Rao, *Chem. Eng. J.*, 2013, **221**, 204–213.
49 B. Zhu, L. Chen, T. Yan, J. Xu, Y. Wang, M. Chen and H. Jiang, *Water Sci. Technol.*, 2018, **78**, 1179–1188.
50 P. Zhang, T. He, P. Li, X. Zeng and Y. Huang, *Langmuir*, 2019, **35**, 13562–13569.
51 Y. Zhang, L. Wang, L. Zou and D. Xue, *J. Cryst. Growth*, 2010, **312**, 3367–3372.
52 L. Bo, Q. Li, Y. Wang, L. Gao, X. Hu and J. Yang, *Environ. Prog. Sustainable Energy*, 2016, **35**, 1420–1429.

53 M. N. Sepehr, K. Yetilmezsoy, S. Marofi, M. Zarrabi, H. R. Ghaffari, M. Fingas and M. Foroughi, *J. Taiwan Inst. Chem. Eng.*, 2014, **45**, 2786–2800.
54 M. R. Berber, I. H. Hafez, K. Minagawa, M. Katoh, T. Mori and M. Tanaka, *J. Mol. Struct.*, 2013, **1033**, 104–112.
55 H. Zhang, G. Zhang, X. Bi and X. Chen, *J. Mater. Chem. A*, 2013, **1**, 5934–5942.
56 U. Costantino, F. Marmottini, M. Nocchetti and R. Vivani, *Eur. J. Inorg. Chem.*, 1998, 1439–1446.
57 M. Shao, F. Ning, J. Zhao, M. Wei, D. G. Evans and X. Duan, *J. Am. Chem. Soc.*, 2011, **134**, 1071–1077.
58 K. Mandel, A. Drenkova-Tuhtan, F. Hutter, C. Gellermann, H. Steinmetz and G. Sextl, *J. Mater. Chem. A*, 2013, **1**, 1840–1848.
59 N. Ammavasi and R. Mariappan, *J. Environ. Chem. Eng.*, 2018, **6**, 5645–5654.
60 R. Zeng, Z. Liu, F. Zhang, S. Li, Q. He, H. Cui and E. Han, *Trans. Nonferrous Met. Soc. China*, 2015, **25**, 1917–1925.
61 J. Shou, C. Jiang, F. Wang, M. Qiu and Q. Xu, *J. Mol. Liq.*, 2015, **207**, 216–223.
62 S. Arghavani-Beydokhti, M. Rajabi and A. Asghari, *Anal. Methods*, 2018, **10**, 1305–1314.
63 W. H. R. Shaw and J. J. Bordeaux, *J. Am. Chem. Soc.*, 1955, **77**, 4729–4733.
64 V. Siva Kumar, A. H. Padmasri, C. V. V. Satyanarayana, I. Ajit Kumar Reddy, B. David Raju and K. S. Rama Rao, *Catal. Commun.*, 2006, **7**, 745–751.
65 F. Loretta, S. Perumal and S. Ramalingom, *Asian J. Chem.*, 2013, **25**, 1921–1926.
66 A. A. Markeb, L. A. Ordosgoitia, A. Alonso, A. Sánchez and X. Font, *RSC Adv.*, 2016, **6**, 56913–56917.
67 E. Mohammadi, H. Daraei, R. Ghanbari, S. Dehestani Athar, Y. Zandsalimi, A. Ziaee, A. Maleki and K. Yetilmezsoy, *J. Mol. Liq.*, 2019, **273**, 116–124.
68 R. Cheng, L. Shen, Y. Zhang, D. Dai, X. Zheng, L. Liao, L. Wang and L. Shi, *Water*, 2018, **10**, 1659.
69 D. Jiang, Y. Amano and M. Machida, *J. Environ. Chem. Eng.*, 2017, **5**, 4229–4238.
70 M. Rashid, N. T. Price, M. Á. Gracia Pinilla and K. E. O'Shea, *Water Res.*, 2017, **123**, 353–360.
71 O. Mrózek, P. Ecorchard, P. Vomáčka, J. Ederer, D. Smržová, M. Š. Slušná, A. Machálková, M. Nevoralová and H. Beneš, *Appl. Clay Sci.*, 2019, **169**, 1–9.
72 M. Gilanizadeh and B. Zeynizadeh, *New J. Chem.*, 2018, **42**, 8553–8566.
73 N. Passe-Coutrin, S. Altenor, D. Cossement, C. Jean-Marius and S. Gaspard, *Microporous Mesoporous Mater.*, 2008, **111**, 517–522.
74 M. Y. Akram, S. Ahmed, L. Li, N. Akhtar, S. Ali, G. Muhyodin, X. Zhu and J. Nie, *J. Environ. Chem. Eng.*, 2019, **7**, 103137.
75 C. Han, J. Lalley, N. Iyanna and M. N. Nadagouda, *Mater. Chem. Phys.*, 2017, **198**, 115–124.
76 J. Liu, J. Cao, Y. Hu, Y. Han and J. Zhou, *Water Sci. Technol.*, 2017, **76**, 2867–2875.
77 J. Wang, X. Shao, J. Liu, Q. Zhang, J. Ma and G. Tian, *Mater. Chem. Phys.*, 2020, **249**, 123024.
78 F. Yang, S. Zhang, Y. Sun, D. C. W. Tsang, K. Cheng and Y. S. Ok, *J. Hazard. Mater.*, 2019, **365**, 665–673.
79 D. Fang, X. Zhuang, L. Huang, Q. Zhang, Q. Shen, L. Jiang, X. Xu and F. Ji, *Sci. Total Environ.*, 2020, **725**, 138490.

 